AD

AD-E403 316

Technical Report ARMET-TR-10020

EFFECT OF PROCESSING PARAMETERS ON THE PHYSICAL, THERMAL, AND COMBUSTION PROPERTIES OF PLASMA-SYNTHESIZED ALUMINUM NANOPOWDERS

Chris Haines
Darold Martin
Deepak Kapoor
Joseph Paras
Ryan Carpenter

February 2011

U.S. ARMY ARMAMENT RESEARCH, DEVELOPMENT AND ENGINEERING CENTER

Munitions Engineering Technology Center

Picatinny Arsenal, New Jersey

REPORT DOCUMENTATION PAGE

Form Approved
OMB No. 0704-01-0188

1. REPORT DATE (DD-MM-YYYY)	2. REPORT TYPE	3. DATES COVERED (*From - To*)
February 2011		October 2008 to September 2009

4. TITLE AND SUBTITLE

EFFECTS OF PROCESSING PARAMETER ON THE PHYSICAL, THERMAL, AND COMBUSTION PROPERTIES OF PLASMA-SYNTHESIZED ALUMINUM NANOPOWDERS

5a. CONTRACT NUMBER

5b. GRANT NUMBER

5c. PROGRAM ELEMENT NUMBER

6. AUTHORS

Chris Hanies, Darold Martin, Deepak Kapoor, Joseph Paras, and Ryan Carpenter

5d. PROJECT NUMBER

5e. TASK NUMBER

5f. WORK UNIT NUMBER

7. PERFORMING ORGANIZATION NAME(S) AND ADDRESS(ES)

U.S. Army ARDEC, METC
Energetics, Warheads & Manufacturing Technology Directorate (RDAR-MEE-M)
Picatinny Arsenal, NJ 07806-5000

8. PERFORMING ORGANIZATION REPORT NUMBER

9. SPONSORING/MONITORING AGENCY NAME(S) AND ADDRESS(ES)

U.S. Army ARDEC, ESIC
Knowledge & Process Management (RDAR-EIK)
Picatinny Arsenal, NJ 07806-5000

10. SPONSOR/MONITOR'S ACRONYM(S)

11. SPONSOR/MONITOR'S REPORT NUMBER(S)

Technical Report ARMET-TR-10020

12. DISTRIBUTION/AVAILABILITY STATEMENT

Approved for public release; distribution is unlimited.

13. SUPPLEMENTARY NOTES

14. ABSTRACT

A design of experiments (DOE) was conducted to determine the effects of processing parameters on the physical, thermal, and combustion properties of nanometer scale aluminum powders prepared via an inductively-coupled plasma (ICP) inert gas condensation method. A four-factor, two-level half-fractional factorial array was developed to minimize the number of experiments. Factors chosen for the DOE were plasma power, system pressure, feed rate, and quench rate. Particle size was chosen as the measured response due to its predominant effect on material properties. The results of the DOE showed that feed rate and quench rate have the largest effect on particle size. All synthesized powders were characterized by thermogravimetric analysis/differential scanning calorimetry; field emission scanning electron microscope, Brunauer, Emmet, and Teller; and bomb calorimetry.

15. SUBJECT TERMS

Nanopowder Synthesis Plasma Aluminum Design of experiments (DOE) Combustion

16. SECURITY CLASSIFICATION OF:			17. LIMITATION OF ABSTRACT	18. NUMBER OF PAGES	19a. NAME OF RESPONSIBLE PERSON
a. REPORT	b. ABSTRACT	c. THIS PAGE			Chris D. Haines
U	U	U	SAR	18	19b. TELEPHONE NUMBER (Include area code) (973) 724-3037

CONTENTS

FIGURES

ACKNOWLEDGMENTS

This research was supported by the Nanotechnology for Future Force Armaments Non-ATO, CORE funding from the Office of the Assistant Technical Director, U.S. Army Armaments Research, Development and Engineering Center, Picatinny Arsenal, New Jersey. The authors also thank Tekna Plasma Systems, Inc. for their continued support and guidance.

INTRODUCTION

Nanoscale powders (primary particle size between 1 and 100 nm) have become the focus of a tremendous amount of research due to their extremely high surface area, which leads to significantly different properties than that of their macroscale counterparts. Materials at t his length scale are known to exhibit unique physical, chemical, optical, electrical, magnetic, and mechanical properties not possible with conventional materials. Nanoscale metals have an additional level of interest in the energetic community due to their inherent pyrophoricity; noble metals being the exception to the rule. The ratio of surface atoms to bulk atoms at this size scale is very high (ref. 1) and leads to enhanced reactivity with oxygen, even at room temperature. Nanoscale aluminum has attracted a considerable amount of attention due to its high combustion enthalpy, making it an excellent candidate for usage in propellants, explosives, and pyrotechnics (refs. 2 to 4). A number of different techniques for production of aluminum nanopowders have been reported including aluminum exploding wire (ref. 5), plasma (ref. 6), and wet chemistry (ref. 7).

This work reports on nanoaluminum synthesized via inductively-coupled plasma (ICP) inert gas condensation. An abbreviated schematic of the process is shown in figure 1. Precursors, in the form of powders or liquids, are injected into the plasma using a dispersion probe. The precursors are completely vaporized and continued downstream into a cold quench gas where the vapors rapidly condense into nanoparticulates. The nanopowders and gases pass through a cyclone separator and eventually lightly deposit onto porous filters. Once a significant pressure differential develops across the wall of the filter, a blowback is used to knock the nanopowders off the filters and down into a collection canister.

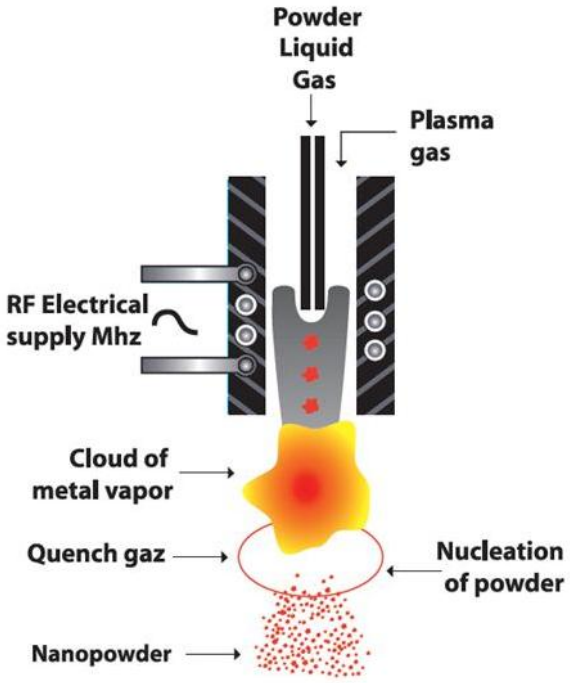

Figure 1
ICP nanopowder synthesis process

Inductively-coupled plasma technology has a number of unique advantages: plasma temperatures exceeding 10,000 Kelvin ensure complete vaporization of feed material; axial feeding of powders into the plasma providing uniform thermal history; no use of electrodes which eliminates contamination issues; and operation under various atmospheres. The ability to use different atmospheres allows tremendous flexibility in synthesizing a wide array of material systems. However, this versatility comes at the cost of having many processing parameters that can be adjusted to control the nanopowder properties. This study examined four of the primary parameters and their effect on the particle size of the powders, which in turn affects the thermal and combustion behavior of the materials. A design of experiments (DOE) was used to systematically assess the influence of each parameter on the particle size of the powder. To minimize the number of experiments, a four-factor, two-level half-fractional fractional array was developed with the factors being feed rate, plasma power, system pressure, and quench rate.

EXPERIMENTAL PROCEDURE

Conventional, micron sized, aluminum powder (Valimet H-10) was selected as the feed material due to its low cost, good flowability, and minimal oxide content. The particle size distribution (PSD) of the as-received powders was measured using a Malvern Instruments Mastersizer/E MAE5000. The size and morphology of the powders were observed on a Zeiss Supra 40VP field emission scanning electron microscope (FE-SEM). It was determined from the results of the PSD and FE-SEM analysis that the powders should be sieved to -325 mesh to remove any large agglomerated powders that could plug the feed probe.

One hundred fifty grams of sieved feed powders were loaded into a vibratory bowl feeder, sealed, and then purged with argon. Teflon tubing was used between the vibratory feeder and the injection probe. An argon/hydrogen mixture (7:1) was used for the plasma gas and pure argon for the quench gas. A small flow (25 mL/min) of pure oxygen was used as a means of in-situ passivation. All gas flow rates were kept constant for all runs, except for the quench gas which was one of the factors in the DOE. Two levels (low/high) were used for each of the factors in the DOE. Quench rates used were 500 slpm and 1100 slpm. Powder feed rates were either at 2 to 3 g/min or 10 to 15 g/min. Plasma power was either 70 kW or 90 kW. Lastly, system pressure was kept at either 10 psi or 15 psi. Powders were fed until the bowl was empty, so actual run time was determined by the feed rate.

All powder collected were subjected to an identical characterization matrix. Surface area was determined on a Quantachrome NOVA2000 Brunauer, Emmet, and Teller (BET) surface area analyzer. X-ray diffraction (XRD), and subsequent crystallite size calculation, was conducted using a Rigaku Ultima X-ray Diffractometer with Jade software. The FE-SEM was used to corroborate primary particle size calculated from BET and XRD crystallite size, as well as analyze the morphology of the powders. Simultaneous thermalgravimetric analysis (TGA) and differential scanning calorimetry (DSC) measurements were made using a Netzsch STA 449 C Jupiter TGA-DSC. Lastly, bomb calorimetry measurements were made using a Parr Bomb Calorimeter.

RESULTS AND DISCUSSIONS

A FE-SEM image of the as-received Valimet H-10 powder can be seen in figure 2, along with the corresponding data from the PSD measurement. The average particle size appears close to that reported by the vendor, d_{50} – 12.5 µm. However, there is also a significant amount of fines, some submicron, seen in the image and PSD data. In general, the powders have a spherical morphology and are only loosely agglomerated, which is likely what leads to their good flowability.

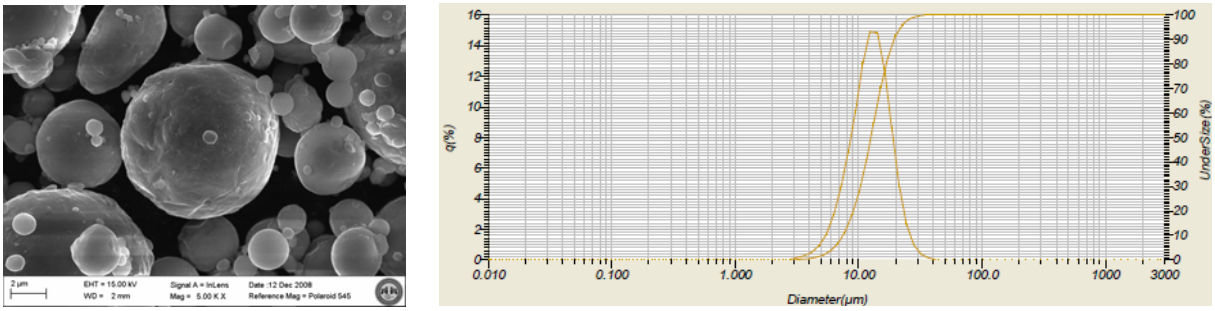

Figure 2
FE-SEM image of the as-received aluminum feed powders (left) and PSD data

The XRD patterns for the as-received and ICP-processed powder are shown in figure 3. The pattern for the nanopowder was chosen at random, but is representative of what was seen in each of the samples from the eight different runs. It is important to note that no aluminum oxide peaks are seen in the plasma-processed powder, suggesting that the inert processing and controlled, in-situ passivation was effective. Also, there is evidence of peak broadening in the nanoscale, ICP-processed powder, as seen in the inset in figure 3. This broadening allowed for calculating the crystallite size for each powder using the Jade software. These values were consistently in good agreement with the values calculated from BET and observed visually with FE-SEM, as seen in table 1.

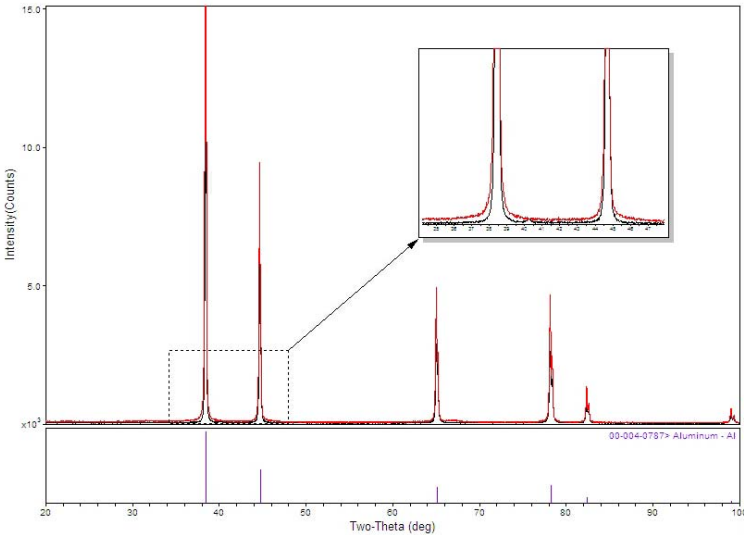

Figure 3
Overlay of XRD patterns from as-received (black) and ICP-processed powder (red)

Table 1
Average particle size determine by XRD, BET, and FE-SEM

Run no.	XRD crystallite size	Average particle size from calculated from BET	Average particle as seen in FE-SEM	Average of three techniques
1	150	164.4	150	154.8
2	225	227.9	220	224.3
3	60	68.4	60	62.8
4	100	104.2	100	101.4
5	150	162.8	160	157.6
6	200	204.8	200	201.6
7	85	79.1	90	84.7
8	100	103.6	100	101.2

The results of the DOE are shown in table 2. As seen in the calculated effect size, the feed rate and quench rate have the largest effect on the particle size of the powders. In comparison, the effect of plasma power and system pressure is negligible. This is best seen with the effects plots shown in figure 4. The effect of the feed rate is strongly positive, meaning that increasing the feed rate will increase the particle size of the powders. Likewise, the effect of the quench rate is strongly negative, meaning that increasing the quench rate will decrease the particle size. This is good agreement with what is seen in practice. The FE-SEM images of the nanopowders processed at various processing conditions are shown in figure 5. Important to note is the greater than three-fold increase in particle size between the extreme conditions; low feed/high quench yielding 60 nm powders and high feed/low quench yielding 200 nm powders. This is an important result as it suggests that the particle size is highly tunable by manipulating only a couple of processing parameters.

Table 2
Statistical results of the DOE

Run no.	Plasma power	Feed rate	System pressure	Quench rate	Test results			Average
1	High	High	High	High	154.8	148.6	149.3	150.9
2	High	High	High	Low	224.3	211.9	218.6	218.2667
3	High	Low	Low	High	62.8	59.8	65.4	62.66667
4	High	Low	Low	Low	101.4	112.9	99.8	104.7
5	Low	High	Low	High	157.6	154.6	145.9	152.7
6	Low	High	Low	Low	201.6	211.1	208.9	207.2
7	Low	Low	High	High	84.7	92.1	90.5	89.1
8	Low	Low	High	Low	101.2	99.7	104.8	101.9
∑+	536.5333	729.0667	560.1667	455.3667				
∑-	550.9	358.3667	527.2667	632.0667				
∑+/n+	134.1333	182.2667	140.0417	113.8417				
∑-/n-	137.725	89.59167	131.8167	158.0167				
Effect	-3.59167	92.675	8.225	-44.175				

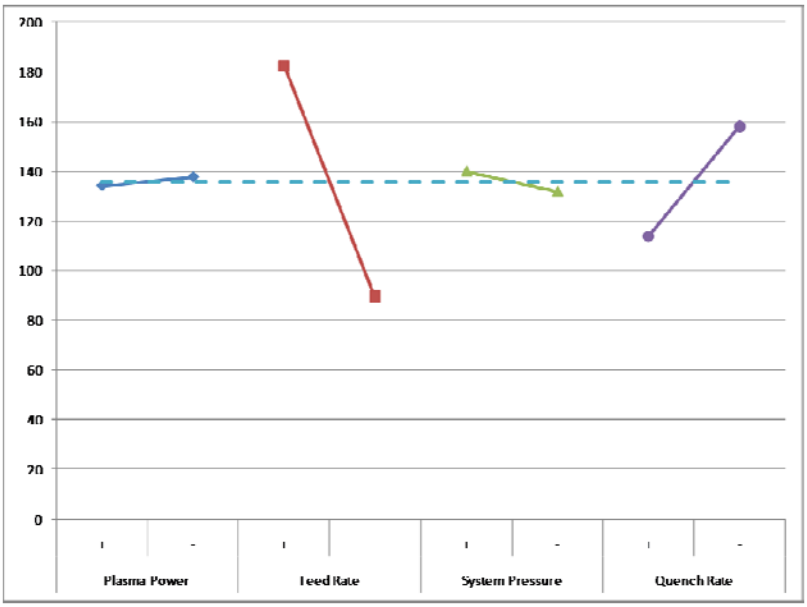

Figure 4
Effects plot showing strong dependence on feed rate and quench rate

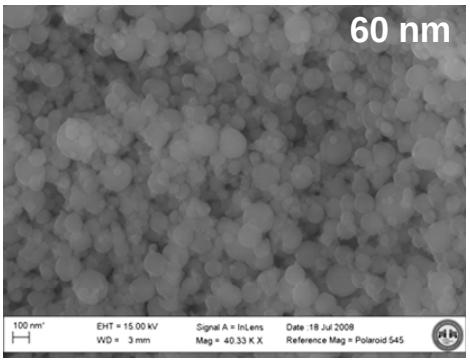

Low feed/high quench

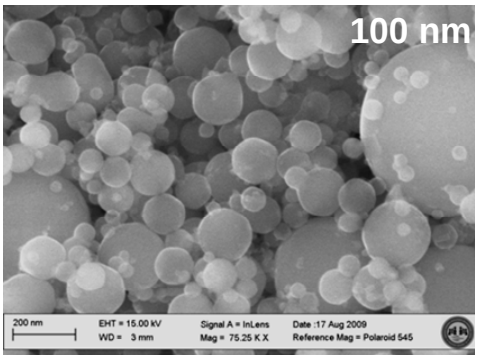

Low feed/low quench

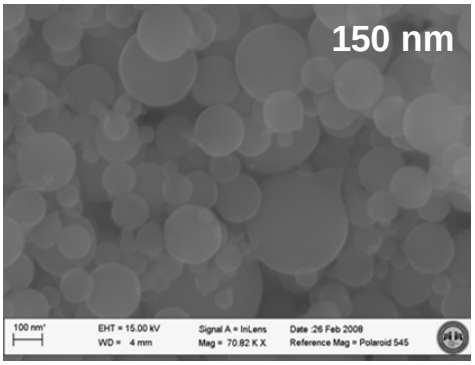

High feed/high quench

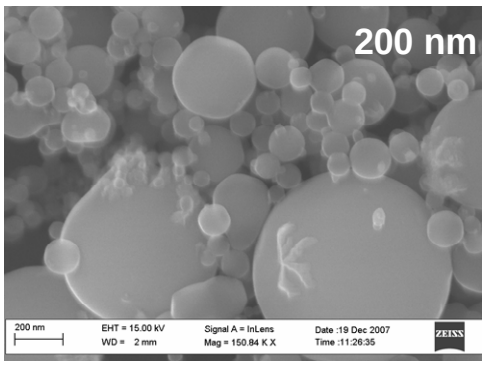

High feed/low quench

Figure 5
FE-SEM images of ICP-processed powder at various conditions

Results from thermal analysis on three different size powders are shown in figure 6. Both the DSC (top) and TGA (bottom) curves show considerable effect of particle size on the thermal properties. The DSC data shows that there are two distinct regions of exothermic activity for each material, one centered just below 600°C and one centered around 800°C. These are both from the oxidation of the Al to form Al_2O_3.

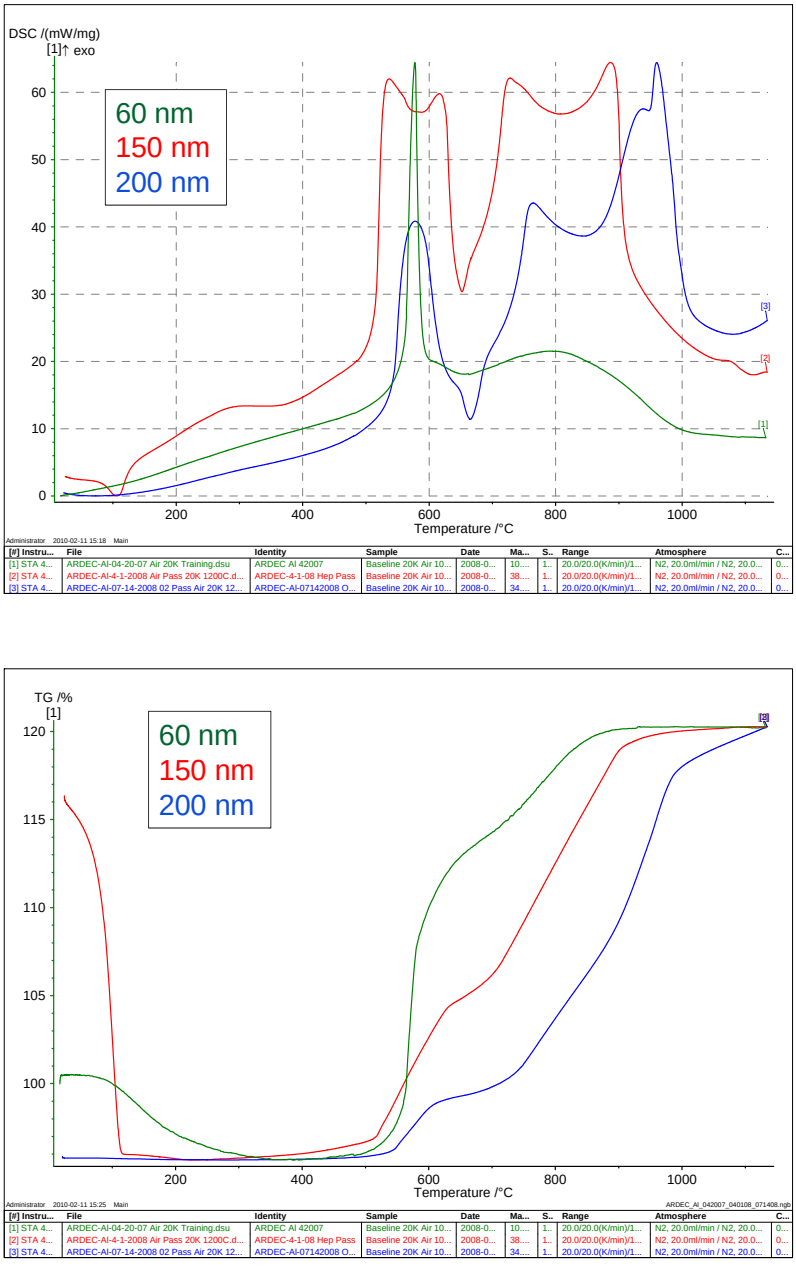

Figure 6
Results of DSC (top) and TGA (bottom) for three different particle size powders

Although a little hard to decipher from the normalized DSC curves, the lower temperature oxidation is most prominent in the smallest particle size powder (60 nm) and becomes less of a contributor with increasing particle size. Likewise, the higher temperature oxidation is most prominent in the larger particle size powders. This can also be seen in the TGA data, where the largest percent weight gain for the 60 nm powder sample occurs below 600°C, while for the larger powders this occurs well above 600°C. This behavior is to be expected since the surface energy and driving force for oxidation is inversely proportional to particle size.

The results of the bomb calorimetry measurements are given in figure 7. The resulting gross heat (MJ/kg) is plotted as a function of the particle size of the powder. The peak gross heat is seen in powders with average particle sizes around the 80 to 100 nm range, falling off considerably with both larger and smaller powders. We expect that this is due to two different phenomena. The decrease in combustion performance with the larger powders is believed to be due to the reduced surface energy which slows down the reaction kinetics. The decrease in the smaller powders is likely the result of the lower weight percent of available aluminum for oxidation. The thickness of the oxide shell on aluminum nanopowder is typically in the 2 to 4 nm range, somewhat independent of particle size. Therefore, as the diameter of the particle decreases, so does the percent of un-reacted aluminum. As an example: assuming an oxide shell thickness of 3 nm, a 100 nm particle would have approximately 83 wt. % of un-reacted aluminum while a 10 nm would contain only about 6 wt. % of un-reacted aluminum.

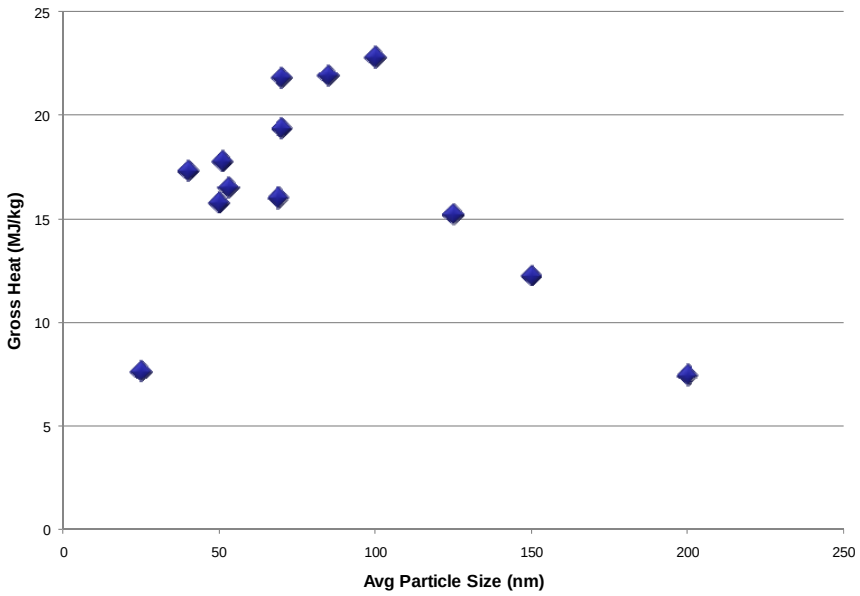

Figure 7
Bomb calorimetry results plotted as a function of particle size

CONCLUSIONS

The results of the design of experiments showed that feed rate and quench rate are the parameters which have the greatest effect on particle size of the powder. In comparison, the system pressure and plasma power were almost negligible. The smallest powders (~60 nm) were synthesized with low feed rate and high quench while the largest powders (~200 nm) we obtained with high feed rates and low quench. The particle size calculations via XRD peak broadening, calculated from Brunauer, Emmet, and Teller surface area, and visual observations with electron microscopy were all in good agreement. The thermal properties of the powders are strongly dependent on the particle size of the powders. The smaller powders oxidize much faster and at lower temperatures (below 600°C) while the larger powders oxidize more gradually at higher temperatures (above 600°C). Lastly, the bomb calorimetry data shows a “sweet spot” for maximum gross heat around 80 to 100 nm, which is consistent with trends seen in the literature.

REFERENCES

1. Klabunde, K. J.; Stark, J.; Koper, O.; et al., J. Phys. Chem. 100, 12142-12153, 1996.

2. Jeurgens, L.P.H.; Sloof, W. G.; Tichelaar, F. D.; and Mittemeijer, E. J., J. Appl. Phys. 92, 1649-1656, 2002.

3. Trunov, M.A.; Schoenitz, M.; Zhu, X.; and Dreizin, E. L., Combust. Flame 140, 310-318, 2005.

4. Sun, J.; Pantoya, M. L.; Simon, S. L., Thermochim. Acta 444, 117-127, 2006.

5. Ivanov, G. V.; Tepper, F., Challenges in Propellants and Combustion: 100 Years After Nobel, K. K. Kuo, et al. (Eds), Begell House, New York, pp. 636-645, 1997.

6. Pivkina, A.; Ivanov, D.; Frolov, Y.; Mudretsova, S.; Nickolskaya, A.; and Schoonman, J., J. Therm. Anal. Calorimetry 86, 733-738, 2006.

7. Jouet, R. J.; Warren, A. D.; Rosenberg, D. M.; Bellitto, V. J.; Park, K.; and Zachariah, M. R., Chem. Mater. 17, 2987-2996, 2005.

DISTRIBUTION LIST

U.S. Army ARDEC
ATTN: RDAR-EIK
RDAR-GC
RDAR-MEE-M (20)
RDAR-MEM-L, M. Donadio
RDAR-MEE-T, J. Wejsa
C. Csernica
J. Poret
J. Sabatini
RDAR-MEE-W, E.Caravaca
E. Rozumov
Picatinny Arsenal, NJ 07806-5000

Defense Technical Information Center (DTIC)
ATTN: Accessions Division
8725 John J. Kingman Road, Ste 0944
Fort Belvoir, VA 22060-6218

Commander
Soldier and Biological/Chemical Command
ATTN: AMSSB-CII, Library
Aberdeen Proving Ground, MD 21010-5423

Director
U.S. Army Research Laboratory
ATTN: AMSRL-CI-LP, Technical Library
Bldg. 4600
Aberdeen Proving Ground, MD 21005-5066

Chief
Benet Weapons Laboratory, WSEC
U.S. Army Research, Development and Engineering Command
Armament Research, Development and Engineering Center
ATTN: RDAR-WSB
Watervliet, NY 12189-5000

Director
U.S. Army TRADOC Analysis Center-WSMR
ATTN: ATRC-WSS-R
White Sands Missile Range, NM 88002

Chemical Propulsion Information Agency
ATTN: Accessions
10630 Little Patuxent Parkway, Suite 202
Columbia, MD 21044-3204

GIDEP Operations Center
P.O. Box 8000
Corona, CA 91718-8000

AFRL/RXLMD
ATTN: Dr. Jonathan Spowart
2230 Tenth St, Ste. 1
Wright-Patterson AFB, OH 45433